Chemical Science

EDGE ARTICLE

View Article Online
View Journal | View Issue

Cite this: *Chem. Sci.*, 2017, **8**, 2436

A new class of Cu/ZnO catalysts derived from zincian georgeite precursors prepared by co-precipitation†

Paul J. Smith,[a] Simon A. Kondrat,[a] Philip A. Chater,[b] Benjamin R. Yeo,[a] Greg M. Shaw,[a] Li Lu,[c] Jonathan K. Bartley,[a] Stuart H. Taylor,[a] Michael S. Spencer,[a] Christopher J. Kiely,[c] Gordon J. Kelly,[d] Colin W. Park[d] and Graham J. Hutchings*[a]

Zincian georgeite, an amorphous copper–zinc hydroxycarbonate, has been prepared by co-precipitation using acetate salts and ammonium carbonate. Incorporation of zinc into the georgeite phase and mild ageing conditions inhibits crystallisation into zincian malachite or aurichalcite. This zincian georgeite precursor was used to prepare a Cu/ZnO catalyst, which exhibits a superior performance to a zincian malachite derived catalyst for methanol synthesis and the low temperature water–gas shift (LTS) reaction. Furthermore, the enhanced LTS activity and stability in comparison to that of a commercial $Cu/ZnO/Al_2O_3$ catalyst, indicates that the addition of alumina as a stabiliser may not be required for the zincian georgeite derived Cu/ZnO catalyst. The enhanced performance is partly attributed to the exclusion of alkali metals from the synthesis procedure, which are known to act as catalyst poisons. The effect of residual sodium on the microstructural properties of the catalyst precursor was investigated further from preparations using sodium carbonate.

Received 14th September 2016
Accepted 29th December 2016

DOI: 10.1039/c6sc04130b

www.rsc.org/chemicalscience

Introduction

Since the early 1960s, $Cu/ZnO/Al_2O_3$ catalysts have been used commercially for methanol synthesis and the LTS reaction. In 2009 worldwide methanol production exceeded 40 million metric tonnes,[1] whilst the LTS process is a key part of the overall process for ammonia production.[2,3] There is now general acceptance that Cu is the active phase for these reactions, and very recent studies have suggested that the primary role of ZnO is to create a strong metal support interaction (SMSI).[4–6] This materials combination permits stabilised Zn-incorporated Cu surfaces to be prepared which are highly defective, and enables the density of the active sites to be optimised. Alumina incorporation into the catalyst is essential for enhancing both catalyst stability and lifetime by suppressing the thermal sintering of the nano-scale Cu crystallites.[7–11] Moreover, many studies suggest that alumina also acts as a promoter, through evidence of Al^{3+} doping into ZnO, which specifically tailors the reduction properties of the latter.[12,13]

The multi-step synthesis of $Cu/ZnO/Al_2O_3$ catalysts was also introduced in the 1960s and whilst it has been fine-tuned and optimised, no major changes in the process have been reported. The initial step comprises the synthesis of a highly mixed CuZn(Al) hydroxycarbonate by co-precipitation. This involves addition of metal nitrate and sodium carbonate solutions at a controlled pH and temperature. The amorphous precipitate initially formed is aged, resulting in the formation of crystalline precursors. This ageing step is widely considered as essential to generate the optimum crystalline hydroxycarbonate precursors from an amorphous phase, that is itself considered to have inferior microstructural characterisitcs.[1,8,12,14–25] However in some cases, non-aged precursors have been shown to illustrate desired microstructural features.[26] Typical crystalline phases obtained range from Cu-rich to Zn-rich compositions in binary preparations and include; malachite $Cu_2(OH)_2CO_3$, zincian malachite $(Cu_xZn_y)_2(OH)_2CO_3$, aurichalcite $(Cu_xZn_y)_5(OH)_6(CO_3)_2$ and hydrozincite $Zn_5(OH)_6(CO_3)_2$. Studies on binary preparations have enabled a greater understanding of the more complex ternary (Cu/Zn/Al) system to be attained. Consequently, zincian malachite is currently considered to be the optimum precursor for the methanol synthesis catalyst. This is attributed to the interwoven, nano-scale needle morphology, which facilitates formation of a highly porous meso-structure.[1,16,20,27,28] The optimum Cu : Zn molar ratio is close to 2 : 1, since 27 at% Zn is the maximum amount which can be substituted into the malachite lattice.[12,16,28] Higher Zn contents are desirable to facilitate further dilution of the Cu

[a]*Cardiff Catalysis Institute, School of Chemistry, Cardiff University, Main Building, Park Place, Cardiff, CF10 3AT, UK. E-mail: hutch@cardiff.ac.uk*

[b]*Diamond Light Source, Didcot, OX11 0DE, UK*

[c]*Department of Materials Science and Engineering, Lehigh University, 5 East Packer Avenue, Bethlehem, Pennsylvania 18015, USA*

[d]*Johnson Matthey, PO Box 1, Belasis Avenue, Cleveland, TS23 1LB, UK*

† Electronic supplementary information (ESI) available. See DOI: 10.1039/c6sc04130b

component, thereby enhancing synergistic interactions, but this results in a phase separated zincian malachite/aurichalcite precursor. However, it should be noted that aurichalcite and hydrotalcite precursors have been reported as being the optimum phases for producing catalysts for the LTS reaction.[29–31] Thermal decomposition of the hydroxycarbonates results in the formation of an intimate mixture of oxides, sometimes together with residual carbonate, and a subsequent *in situ* reduction step is required to obtain the active catalyst.

We have recently focussed attention on the amorphous georgeite hydroxycarbonate, which has been largely neglected as a catalyst precursor due to its extreme rarity and the relative difficulty of its preparation. Georgeite is formed as a precipitate initially in the preparation of malachite, but only as a transient phase as it rapidly transforms into malachite. It is known that Zn can be incorporated into georgeite to form zincian georgeite, indicating that it could be a suitable catalyst precursor. However, its rarity has meant that only a limited number of studies on this aspect have been published to date.[32–35] We have recently shown that disordered zincian georgeite can be readily synthesised using a specialised supercritical anti-solvent precipitation method, and this enables the preparation of a new class of Cu/ZnO catalysts which give catalytic performances that rival, or even exceed in some instances, those of catalysts prepared from crystalline hydroxycarbonates phases.[36] We have now extended this study and have prepared zincian georgeite by a more amenable co-precipitation method and tested its applicability as a catalyst precursor for methanol synthesis and the LTS reaction. To obtain zincian georgeite, the standard co-precipitation procedure was deliberately modified to avoid the utilisation of nitrates and Na^+, which can lead to residual catalyst poisons being retained and crystalline malachite phases being formed.[14,37,38]

Experimental

Copper–zinc hydroxycarbonates were prepared by a continuous pH co-precipitation procedure as follows: a mixed $Cu(II)(OAc)_2 \cdot H_2O$ (0.35 M) and $Zn(II)(OAc)_2 \cdot 2H_2O$ (0.175 M) solution was prepared using deionised water to give a nominal Cu : Zn molar ratio of 2 : 1. This solution was pre-heated along with a separate aqueous solution of either $(NH_4)_2CO_3$, $(NH_4)HCO_3$ or Na_2CO_3 (0.55 M). The hydroxycarbonates were precipitated by combining these two solutions simultaneously at 40 °C, whilst the pH was held constant at 6.5–7.0. The precipitates were left to age for 15 min, with the blue mother liquor solution left stirring at constant temperature (40 °C). After ageing the precipitates were collected by filtration, washed with deionised water (*ca.* 1 L, 25 °C) and then dried at 40 °C for 16 h in a vacuum oven. For comparative purposes, copper–zinc hydroxycarbonates were also made as follows by the conventional co-precipitation procedure.[1] Mixed $Cu(NO_3) \cdot xH_2O$ and $Zn(NO_3) \cdot xH_2O$ (total concentration = 1.5 M) aqueous solutions were prepared, either with nominal Cu/Zn molar ratios of 2 : 1 or 1 : 1, and pre-heated along with a separate aqueous solution of Na_2CO_3 (1.5 M). Hydroxycarbonates were precipitated by combining these two solutions simultaneously at 65 °C, whilst the pH was held constant at 6.5–6.8. The precipitates were aged for 30 min at 65 °C where a characteristic colour change of the mother liquor solution from blue to green was observed. The hydroxycarbonates were collected by filtration and washed with deionised water (*ca.* 6 L, 65 °C) in order to minimise their sodium content. A photometer was used to determine the point at which there was no further change in sodium content with washing. The samples were then dried at 110 °C for 16 h. Further details regarding catalyst preparation are provided in the ESI.†

Conventional X-ray diffraction (XRD) analysis of the materials produced was performed on a (θ–θ) PANalytical X'pert Pro powder diffractometer with a Ni filtered CuK_α radiation source operating at 40 keV and 40 mA. Patterns were recorded over the 2θ angular range 10–80° using a step size of 0.016°. Synchrotron partial distribution functions (PDF) were derived from XRD data collected on the 11-ID-B beamline at the Advanced Photon Source at Argonn National Laboratory, USA. Powder samples were packed into Kapton capillaries having an internal diameter of 1 mm. Room temperature powder XRD data were collected at a wavelength of 0.2114 Å using the Rapid Acquisition PDF method. The scattering data ($0.5 \leq Q \leq 22$ Å^{-1}) was processed into a PDF using the program GudrunX.

Fourier transform infra-red (FT-IR) spectroscopy on the materials was performed on a Jasco 660 plus spectrometer operating in transmission mode over the range 400–4000 cm^{-1}. Raman spectroscopy was performed using a Renishaw inVia microscope with a green argon ion laser ($\lambda = 514$ nm).

Scanning electron microscopy (SEM) and Energy-dispersive X-ray (EDX) analysis was performed using a Carl Zeiss Evo 40 microscope, operated at 5–20 kV and 50–2000 pA. Analysis was performed by dispersing catalysts on adhesive carbon discs, mounted on 12.5 mm aluminium stubs. 20 × 20 μm scan areas were carried out for quantification on more than 20 particles, with the standard deviation ± 1 at%. Materials for examination by scanning transmission electron microscopy (STEM) were dry dispersed onto a holey carbon TEM grid. These supported fragments were examined using BF- and HAADF-STEM imaging mode in an aberration corrected JEOL ARM-200CF scanning transmission electron microscope (STEM) operating at 200 kV. 55 HAADF- and BF-pairs were collected for each sample analysed. This microscope was also equipped with a Centurio silicon drift detector (SDD) system for energy dispersive X-ray spectroscopy analysis.

Microwave plasma atomic emission spectroscopy (MP-AES) was performed using a 4100 MP-AES manufactured by Agilent Technologies. Solid samples and effluents were digested in 20 vol% HNO_3/H_2O solutions and compositions quantified against calibration standards.

Thermal gravimetric analysis (TGA) and differential thermal analysis (DTA) was performed using a Setaram Labsys 1600 instrument. Samples (20–50 mg) were loaded into alumina crucibles and heated to 600 °C (at 1 or 5 °C min^{-1}) in a flow of synthetic air (50 ml min^{-1}). TGA and evolved gas analysis (EGA) were also run on a Pyris 1 TGA linked to a Perkin Elmer Frontier, followed by a Clarus 580 GC-MS, using a TL-9000 interface. TGA was performed under helium, from 30–600 °C (at 5 °C min^{-1})

using *ca.* 25 mg of sample. For all specified TGA runs, blank runs were subtracted from the relevant data to remove buoyancy effects.

Brunauer Emmett Teller (BET) surface area and porosity analysis was performed using a Quantachrome Autosorb-1.80 point isotherms were obtained using N_2 at −196 °C. Surface area analysis was carried out using an 8 point BET plot in the P/P_0 range 0.06–0.35. Total pore volume and size distributions were calculated from the entire adsorption isotherm using the density functional theory (DFT) Monte–Carlo model. The N_2–silica adsorption branch at −196.15 °C was the kernel file chosen for this DTF analysis.

Cu surface area analysis and CO_2 temperature-programmed desorption (CO_2-TPD) were carried out on a Quantachrome ChemBET chemisorption analyser equipped with a thermal-conductivity detector (TCD). Calcined samples (100 mg) were reduced to catalysts using 10% H_2/Ar (30 ml min^{-1}) with heating to 140 °C at 10 °C min^{-1}, and then to 225 °C at 1 °C min^{-1}. For Cu surface area analysis, catalysts were cooled to 65 °C under He for N_2O pulsing. 12 N_2O pulses (113 μl each) were followed with 3 N_2 pulses for calibration. The amount of N_2 emitted was assumed to amount to half a monolayer coverage of oxygen and that the surface density of Cu is 1.47×10^{19} atoms/m^2. For CO_2-TPD analysis, catalysts were cooled to ambient temperature under He before being exposed to CO_2 (50 ml min^{-1}) for 30 min. Desorption was then performed by heating from 25 to 600 °C at 10 °C min^{-1}, before holding for 20 min under a flow of helium (80 ml min^{-1}).

For catalyst testing, 0.5 g of each catalyst precursor was used after being calcined in air (300 °C, 1 °C min^{-1}, 4 h), pelleted and ground to a sieve fraction diameter of 0.6–1.0 mm. Catalysts were produced by *in situ* reduction by heating to 225 °C at 1 °C min^{-1} using a 2% H_2/N_2 gas mixture (60 ml min^{-1}). Methanol synthesis testing was performed in a single stream six-fixed bed reactor with an additional by-pass line. Catalysts were subjected to synthetic syngas ($CO : CO_2 : H_2 : N_2$ composition = 6 : 9.2 : 67 : 17.8 mol%) at 3.5 L h^{-1}, 25 bar pressure at either 190 or 205 °C. Carbon moles balances were ≥98%. LTS testing was performed in a parallel fixed bed reactor with a single stream feed and an additional by-pass line. Catalysts were subjected to synthetic syngas and vaporised water ($H_2O : CO : CO_2 : H_2 : N_2$ = 50 : 2 : 8 : 27.5 : 12.5 mol%) at 27.5 bar pressure and 220 °C. For both reactions, in-line gas analysis was performed using an FT-IR spectrometer. Total system flows were maintained using a by-pass line. Commercial catalysts for methanol synthesis and the LTS reaction were used as standards and have been described elsewhere.[3,41]

Results and discussion

FT-IR spectroscopy was carried out on the prepared hydroxycarbonates to qualitatively analyse the phases present (Fig. 1A). The spectra of the materials prepared at 40 °C using metal acetates, regardless of the precipitant, can be assigned to zincian georgeite.[14,36] The broad band centred at 3419 cm^{-1} is associated with the O–H stretch, whilst carbonate peaks are present as the intense doublet at 1475 and 1408 cm^{-1} for the ν_3 asymmetric stretch, the weakly visible peak at 1049 cm^{-1} for the ν_1 symmetric stretch and at 836 cm^{-1} for the ν_2 bending mode. As expected, XRD showed no discernible reflections for these samples, as zincian georgeite is known to be amorphous (Fig. 1B). In contrast, the materials produced from preparations carried out at 65 °C with an extended ageing time, were shown by FT-IR and XRD in Fig. 1 to be a phase mixture of zincian malachite and aurichalcite.[14,42] Rietveld refinement determined the aurichalcite content to be *ca.* 10% in the 2 : 1 sample, but was the major phase in the 1 : 1 material.

These findings show that utilisation of lower temperatures and shorter ageing times prevented the ageing of the initial, meta-stable zincian georgeite precipitate into zincian malachite and aurichalcite phases. Phase transformation during ageing requires the presence of water and proceeds *via* a solution and recrystallization mechanism,[15,25] whilst the rate at which ageing occurs increases with temperature. Consequently, this makes

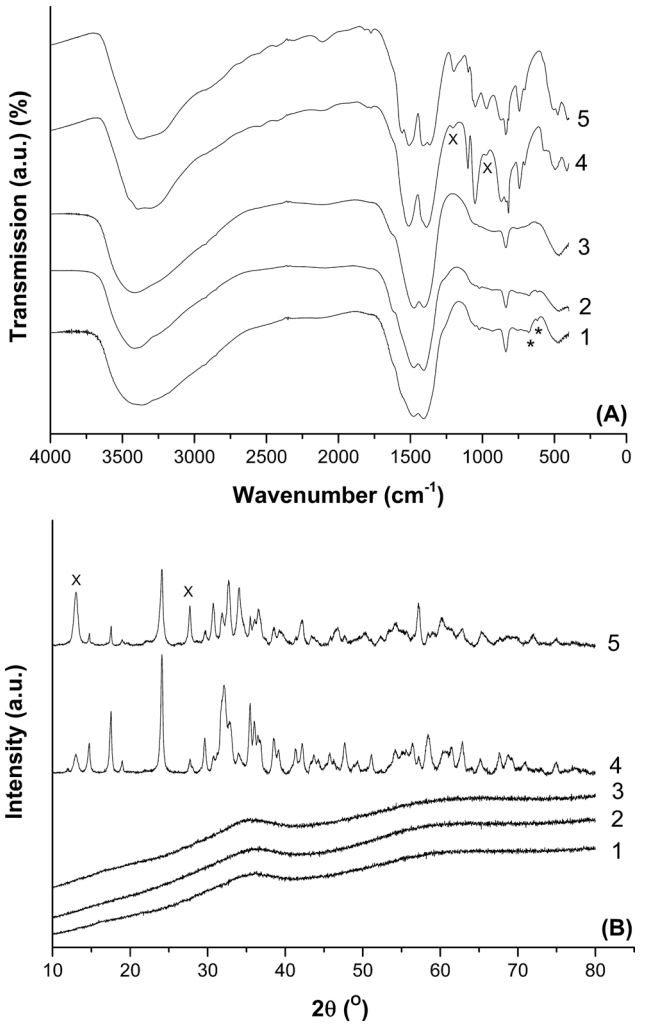

Fig. 1 (A) FT-IR spectra and (B) XRD patterns of 2 : 1 Cu : Zn hydroxycarbonates prepared at 40 °C using metal acetates and (1) $(NH_4)_2CO_3$ (2) NH_4HCO_3 or (3) Na_2CO_3. Metal nitrates and Na_2CO_3 were also used to prepare hydroxycarbonates at 65 °C with Cu : Zn molar ratios of (4) 2 : 1 and (5) 1 : 1. For clarity, metal acetate bands (*) and aurichalcite bands/reflections (X) are marked.

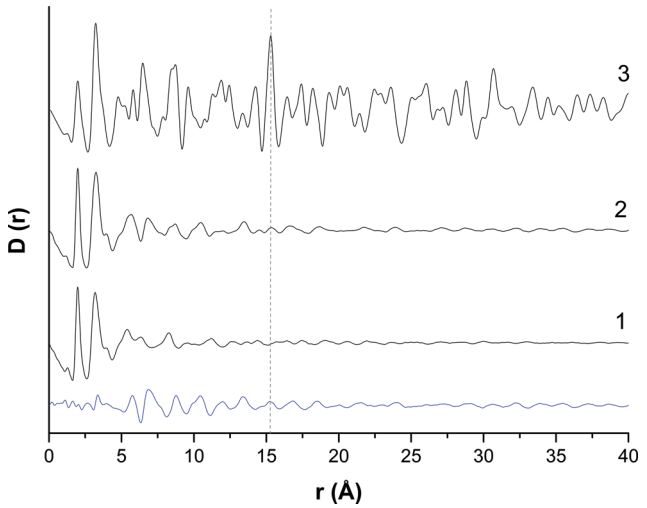

Fig. 2 Observed PDF $D(r)$ data of zincian georgeite (nominal Cu : Zn molar ratio of 2 : 1) prepared by (1) SAS and (2) co-precipitation. Calculated X-ray PDF data of zincian malachite (nominal Cu : Zn molar ratio of 4 : 1) is also provided (3). The hashed line represents a contribution from crystallographically equivalent copper atoms in neighbouring zincian malachite unit cells. The blue difference curve represents structural differences between the SAS and co-precipitated zincian georgeite materials.

preparation of georgeite hydroxycarbonates very difficult when using industrial co-precipitation conditions, primarily because of the higher temperatures used. Whilst the observation of a colour change of the mother liquor solution from blue to green is an indication that ageing has occurred, the simultaneous release of CO_2 during this phase change has also been reported.[15] This is in agreement with our previous findings that zincian georgeite has a higher (CO_3) : (Cu + Zn) ratio than mixed zincian malachite/aurichalcite materials.[36] We also found that when Zn was excluded from the preparations, the georgeite formed rapidly aged into malachite, even when attempts were made to instantly isolate and dry the precipitate. Hence the presence of Zn enhances the stability of the resulting georgeite phase, and this also supresses the transformation into crystalline phases,[15] albeit only at very mild conditions.

The amorphous nature of the zincian georgeite material was examined further by PDF analysis (Fig. 2). A comparison was made against supercritical CO_2 anti-solvent (SAS) precipitated zincian georgeite, previously reported,[36] as well as a simulated PDF of zincian malachite. The PDFs of the SAS and co-precipitated zincian georgeite samples are similar, albeit with slightly more order obtained from using the co-precipitation route. This structural difference could be associated with a higher impurity content or because the level of supersaturation achieved by co-precipitation is lower than that achieved in the SAS preparation, which may facilitate the formation of slightly more ordered materials. A subtraction of the PDF's also concluded that the main structural deviations occur in the range 5–15 Å, where contributions from second and third coordination spheres are apparent. A comparison of the PDFs for zincian georgeite with that of crystalline zincian malachite shows that these materials all have moderately similar structures up to distances of 5 Å. In each case a single M–O (M = metal) peak was identified with a bond length of 1.98 Å. The presence of a secondary peak is not possible since the inclusion of Zn into these samples reduces the Jahn–Teller distortions of the MO_6 octahedra. Evidence of M–M (3.20–3.24 Å) and C–O bonds (1.16–1.28 Å) were also present at similar distances in this region. However, at distances greater than 5 Å significant differences between zincian georgeite and zincian malachite become apparent, with little order present in the zincian georgeite materials at distances greater than 15 Å. A noteworthy distance at 15.27 Å seen in the zincian malachite sample is associated with crystallographically equivalent Cu atoms. The absence of this in the SAS zincian georgeite indicates no repeating unit cells associated with zincian malachite, while its slight presence in the co-precipitated sample indicates trace contamination with zincian malachite.

In our previous studies on zincian georgeite materials prepared by the SAS method,[36] scanning transmission electron microscopy (STEM) revealed that the zincian georgeite was not completely amorphous. In fact, the amorphous matrix, which contains carbonate and hydroxyl species, also had approximately 10 vol% fraction of sub-2 nm crystalline CuO and Cu_2O particles that were below the detection limit of the X-ray based characterization techniques employed. Hence, STEM studies were also carried out on the zincian georgeite material prepared by co-precipitation with $(NH_4)_2CO_3$, of which representative bright field (BF) and high angle annular dark field (HAADF) images are presented in Fig. 3. The co-precipitated material consists of 1 μm scale agglomerates of 'amorphous' primary particles that are about 200 nm in size (Fig. 3A and B). When viewed at high magnification (Fig. 3C–F) it is clear that a distribution of disconnected *ca.* 2 nm crystalline particles are once again present within the amorphous matrix, whose lattice fringe spacings and interplanar angles are consistent with those expected from CuO or Cu_2O. Hence, on the nanoscale, the SAS and co-precipitated zincian georgeite materials show essentially the same characteristic features in STEM images, with the latter showing a slightly higher volume fraction of nanocrystalline inclusions. It should be noted that both zincian georgeite materials are quite distinct from precursors derived from zincian malachite, which are well known to be much more crystalline in nature.[36] This precursor in comparison exists as 100–200 nm scale agglomerates of more regularly shaped and facetted particles from the outset, that are 20–60 nm in size (ESI Fig. 1A†). Closer examination by BF-STEM imaging (ESI Fig. 1B†) shows the existence of extended lattice fringes in these co-precipitated Cu/Zn malachite grains, as well as the presence of some smaller faint (2 nm) unidentified nanoparticles.

Interestingly, Raman spectroscopy did show the presence of an additional phase in zincian georgeite (ESI Fig. 2†). Carbonate bands were identified at 1091 cm^{-1} from the ν_1 symmetric stretch and at 771 and 724 cm^{-1} corresponding to the ν_4 bending modes. However, intense acetate bands were apparent at 2934 and 938 cm^{-1}, which are assigned as the ν(C–H) and ν(C–C) modes, respectively. Acetate bands at 617 and 678 cm^{-1}, assigned as the $\pi(COO)^-$ and $\alpha(COO)^-$ modes were also present

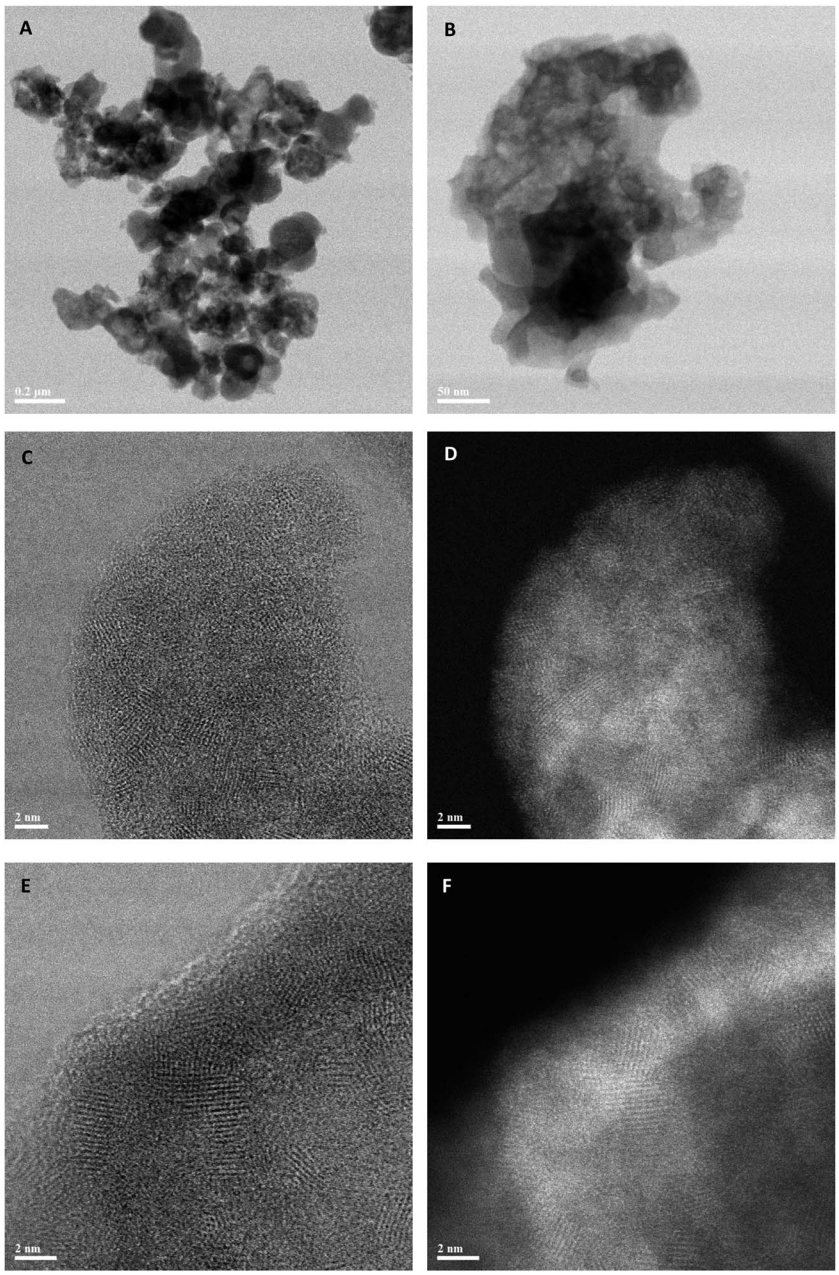

Fig. 3 Representative BF-STEM (A, B, C, E) and HAADF-STEM (D, F) images of the zincian georgeite material prepared by co-precipitation using $(NH_4)_2CO_3$ as the precipitant.

Table 1 EDX and MP-AES analysis to determine Cu : Zn molar ratios and zincian georgeite product yields

Phase(s)	Precipitation reagent	Bulk atomic (%)		Cu/Zn molar ratio	Effluent concentration (mg L^{-1})		Yield (%)	
		Cu	Zn		Cu	Zn	Cu	Zn
Zincian georgeite	$(NH_4)_2CO_3$	64	36	1.8 : 1	430.5	0	92.5	0
	$(NH_4)HCO_3$	64	36	1.8 : 1	222.5	0	96.1	0
	Na_2CO_3	67	33	2 : 1	—	—	—	—
Zincian malachite/aurichalcite	Na_2CO_3	67	33	2 : 1	—	—	—	—
	Na_2CO_3	50	50	1 : 1	—	—	—	—

Table 2 Methanol productivity data for the various catalysts

	MeOH space time yield (S.T.Y.)			
	$mol_{MeOH}\ h^{-1}\ kg_{cat}^{-1}$		$mol_{MeOH}\ h^{-1}\ kg_{Cu}^{-1}$	
Catalyst	190 °C	205 °C	190 °C	205 °C
Zincian georgeite derived[a]	3.19	4.46	5.23	7.31
Zincian malachite derived[b]	2.59	—	4.25	—
Commercial standard[c]	3.64	6.01	7.58	12.51

[a] Catalyst composition by CuO/ZnO wt% = 64 : 36. [b] Catalyst composition by CuO/ZnO wt% = 67 : 33. [c] Catalyst composition by $CuO/ZnO/Al_2O_3$ wt% = 60 : 30 : 10.

in the FT-IR spectra (Fig. 1). This also highlights the difficulty in preparing zincian georgeite of high purity by co-precipitation, since attempts to remove impurities by washing also risks potentially ageing and crystallising the precipitate. In contrast for the zincian malachite/aurichalcite materials, all bands identified were assigned to carbonate,[43,44] suggesting no additional phases were present.

SEM-EDX analysis was carried out on all the prepared hydroxycarbonates to determine the Cu : Zn molar ratios (Table 1). Nominal compositions were achieved from all the preparations which used Na_2CO_3 as a precipitant. However, Cu deficient precursors with Cu : Zn molar ratios of 1.8 : 1 were achieved when using ammonium based reagents. This has also been reported in related studies,[37,38] whereby loss of metal is attributed to a leaching effect, caused by simultaneous formation of a blue copper–amine complex within the mother liquor. To get an estimate of the amount of metal lost from leaching, the resulting blue effluents were collected and analysed by MP-AES (Table 1). It was determined that *ca.* 10 at% of the initial Cu content was lost from leaching but with no loss of Zn.

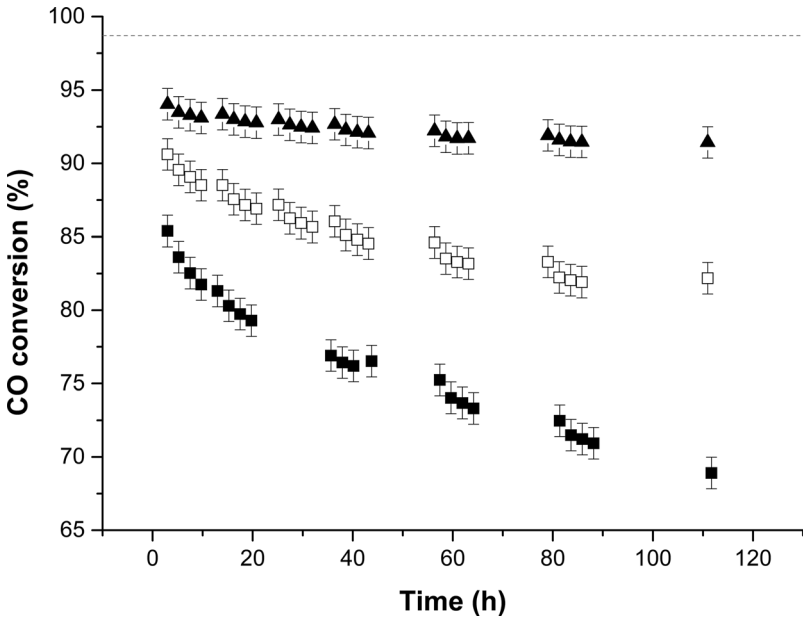

Fig. 4 Time-on-line LTS testing at 220 °C. The grey hashed line represents the maximum conversion due to reaching equilibrium. Key: (black triangles) zincian georgeite derived, (black squares) zincian malachite derived and (open squares) the commercial standard. The nominal compositions of catalysts by wt% was 64 : 36 CuO/ZnO, 67 : 33 CuO : ZnO and 50 : 33 : 17 $CuO/ZnO/Al_2O_3$ for these three catalysts respectively.

Table 3 MP-AES analysis of the various calcined materials to determine effect of precipitant identity and washing treatment on resultant Na loadings

Phase(s)	Precipitation reagent	Washing details	Na weight loading (%)	$mg_{(Na)}\ kg_{(CuO/ZnO)}^{-1}$
Zincian georgeite	$(NH_4)_2CO_3$	1 L water (25 °C)	0.02	148
		N/A	0.02	208
	$(NH_4)HCO_3$	1 L water (25 °C)	0.02	148
		N/A	0.03	340
	Na_2CO_3	1 L water (25 °C)	0.59	5885
		N/A	7.03	70 325
Zincian malachite/aurichalcite	Na_2CO_3	1 L water (65 °C)	0.07[a]	695[a]
	Na_2CO_3	1 L water (65 °C)	0.04[b]	425[b]

[a] Composition by CuO/ZnO wt% = 67 : 33. [b] Composition by CuO/ZnO wt% = 50 : 50.

Interestingly, the findings also indicated a subtle decrease in the loss of Cu by decreasing the amount of ammonia present in solution when using $(NH_4)HCO_3$ as an alternative precipitant.

Zincian georgeite prepared using the supercritical anti-solvent technique has been shown previously to be an excellent precursor for highly active methanol synthesis and LTS catalysts.[36] The activity, stability and selectivity of catalysts derived from zincian georgeite prepared by our modified co-precipitation technique were therefore also evaluated for methanol synthesis and the LTS reaction. A zincian georgeite derived catalyst made using $(NH_4)_2CO_3$ was compared against a zincian malachite/aurichalcite derived catalyst prepared using Na_2CO_3, both having the same nominal CuO/ZnO composition of 2 : 1. Comparisons were also made against the corresponding $Cu/ZnO/Al_2O_3$ catalysts routinely used in industry for these reactions. For methanol synthesis, the zincian georgeite derived catalyst was found to be 20% more active than the zincian malachite/aurichalcite derived catalyst at 190 °C (Table 2). This was slightly more pronounced for the catalyst activities normalised to copper mass. The zincian georgeite derived catalyst was also almost as active as the industrial standard. To investigate this further these catalysts were also tested at 205 °C where the alumina promoted technical catalyst is more resistant to Cu sintering. The higher activity displayed by the industrial catalyst was even more apparent when considering the Cu mass normalised data, and illustrates the significant enhancement in catalyst performance for methanol synthesis when alumina is added to the catalyst.[7,8,11] For comparison, the zincian georgeite derived catalyst prepared by the SAS method achieves MeOH space time yields of 3.92 $mol_{MeOH}\ h^{-1}\ kg_{cat}^{-1}$ at 190 °C and 5.43 $mol_{MeOH}\ h^{-1}\ kg_{cat}^{-1}$ at 205 °C. This demonstrates some enhancement in methanol synthesis activity when using zincian georgeite precursors prepared *via* SAS precipitation as compared to the simpler co-precipitation route described here. We also found a small series of by-phases produced for all the catalysts tested (ESI Fig. S3†). The trace levels of these impurities is consistent for Cu/ZnO catalysts being >99% selective for methanol synthesis.[17]

For the LTS reaction, the catalyst derived from zincian georgeite exceeded the performance of both the zincian malachite derived catalyst and the LTS commercial standard, in terms of both stability and activity (Fig. 4 and ESI Fig. 4†). After 135 h the CO conversions decreased by 3.6, 16.5 and 11% respectively for these catalysts. This illustrates differences in the catalyst deactivation mechanism for MeOH synthesis and the LTS reaction, which cannot simply be attributed to thermal sintering. The promotional effect of alumina is likely tailored to suit these specific reaction conditions. All of the catalysts also produced trace levels of methanol as by-product as methanol synthesis is the primary side reaction (ESI Table S1†). Slightly higher ppm levels were obtained for the zincian georgeite derived catalyst as it produced more CO_2 from the LTS process, which subsequently pushes the equilibrium towards methanol formation. It should also be noted that the SAS prepared zincian georgeite catalyst displays improved LTS activity and stability in comparison to the zincian georgeite derived catalyst prepared by co-precipitation. The CO conversion was 4% higher for the SAS prepared zincian georgeite catalyst and only deactivated by 1% after 112 h. Despite this, the newly developed co-precipitation method described here, is a cheaper and more sustainable preparation route for zincian georgeite, and probably represents a more economically realistic industrial alternative to

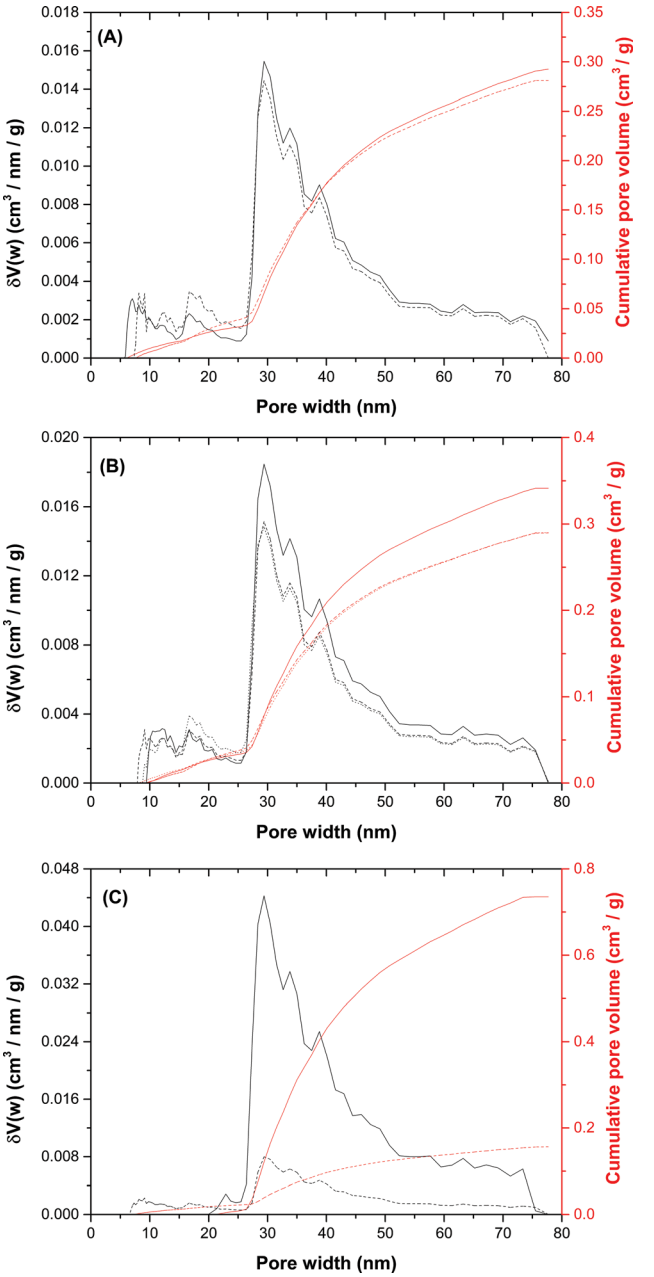

Fig. 5 DFT pore size distributions (black) and cumulative pore volumes (red) of catalyst precursors before and after calcination. (A) Comparison of metal hydroxycarbonates : zincian georgeite prepared using $(NH_4)_2CO_3$ at 40 °C (solid lines) and zincian malachite inc. ~10 wt% aurichalcite prepared using Na_2CO_3 at 70 °C (dotted lines). (B) Calcined zincian georgeite that was prepared using $(NH_4)_2CO_3$ with (solid lines) and without (hashed lines) washing. For comparison, data on calcined zincian malachite inc. ~10 wt% aurichalcite is also provided (dotted lines). (C) Calcined zincian georgeite that was prepared using Na_2CO_3 with (solid lines) and without (hashed lines) washing.

conventional $Cu/ZnO/Al_2O_3$ catalysts made from zincian malachite and aurichalcite.

We then attempted to identify key microstructural differences in the zincian georgeite and zincian malachite derived catalysts in order to rationalise their performances and gain further insight into the design of further optimised catalysts. A contributing factor to the differing impurity contents of these hydroxycarbonates was due to the reagents used in the preparations. Residual nitrates and alkali cations have been reported as catalyst poisons[14,37–40] so MP-AES analysis was used to determine the effect of both the precipitant and the washing procedure directly after co-precipitation on the amount of residual Na^+ (Table 3). Our findings show that residual Na^+ is present in all the materials even when Na_2CO_3 is avoided in the preparation. Despite this, the catalyst derived from zincian georgeite and prepared by co-precipitation using $(NH_4)_2CO_3$ or $(NH_4)HCO_3$ had 148 $mg_{(Na)}\ kg_{(CuO/ZnO)}^{-1}$ as compared to 695 $mg_{(Na)}\ kg_{(CuO/ZnO)}^{-1}$ for the best zincian malachite derived catalyst. The microstructural characteristics of the zincian georgeite and zincian malachite/aurichalcite hydroxycarbonates used in the catalyst tests were then examined, as well as after calcination (300 °C, 1 °C min^{-1}, 4 h) and in the final activated state. Interestingly, DFT porosity analysis determined that both these materials had similar total pore volumes and pore size distributions (Fig. 5A). The BET surface area values were 35 and 27 $m^2\ g^{-1}$ respectively (Table 4). Analysis also showed that the BET surface area and porosities were still similar after calcination (Fig. 5B) as were the Cu surface area values for the final state catalysts (Table 4). These findings indicate that the desired porous mesostructure associated with the malachite phase can also be produced in georgeite derived materials without the need for an ageing step. We next analysed the microstructural evolution of the zincian georgeite prepared using Na_2CO_3 in order to examine the effect of residual Na^+ loadings on the microstructural properties of the material (Fig. 5C). By reducing the Na^+ content from 7 to 0.6% (Table 3) the BET surface area significantly increased from 16 to 56 $m^2\ g^{-1}$ after calcination, whilst the Cu surface area in the resulting catalyst increased from 3 to 21 $m^2\ g^{-1}$ (Table 4).

We performed XRD analysis on all the calcined materials to shed additional light on their microstructural properties (Fig. 6). Washing, followed by calcination resulted in the disordered nature of the zincian georgeite being largely retained, regardless of the precipitant type used. However some weak, ill-defined CuO-type reflections also became evident, indicating crystallite sizes ≤5 nm. In contrast, crystalline materials were always formed in the absence of washing. All reflections in these unwashed calcined materials can be assigned to CuO and ZnO phases with crystallite sizes ≥7 nm. For the zincian malachite/aurichalcite sample, it was not possible to definitely assign metal oxide reflections because of overlap with the numerous zincian malachite and aurichacite reflections still present. In fact, little change was observed in the XRD pattern from the latter conventional materials after calcination, except for a subtle decrease in the peak intensities. Interestingly, Baltes and co-workers have reported that poorly crystalline materials after calcination are required for optimum catalyst performance.[8]

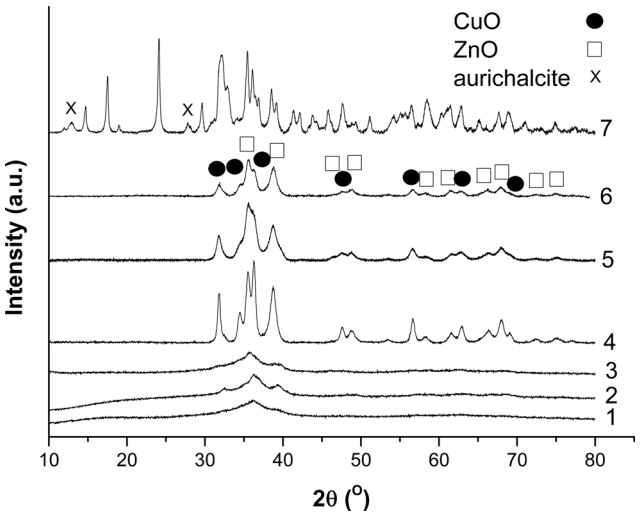

Fig. 6 XRD patterns of the calcined zincian georgeite materials prepared using: (1) $(NH_4)_2CO_3$ (washed), (2) $(NH_4)HCO_3$ (washed), (3) Na_2CO_3 (washed), (4) $(NH_4)_2CO_3$ (no wash), (5) $(NH_4)HCO_3$ (no wash), and (6) Na_2CO_3 (no wash). For comparative purposes, the calcined zincian malachite/aurichalcite material (7) is also presented. All unmarked reflections are associated with the zincian malachite or aurichalcite phases.

Representative STEM micrographs of the co-precipitated zincian georgeite material (prepared using $(NH_4)_2CO_3$) after it had been calcined at 300 °C are presented in Fig. 7. Lower

Table 4 Microstructural properties of metal hydroxycarbonates before and after calcination treatment

Phase(s)	Precipitation reagent	Washing step	Stage of synthesis	BET surface area ($m^2\ g^{-1}$)	Pore volume ($cm^3\ g^{-1}$)	CuO cryst. size (nm)	ZnO cryst. size (nm)	Cu surface area ($m^2\ g^{-1}$)	Cu surface area ($m^2\ g_{Cu}^{-1}$)
Zincain georgeite	$(NH_4)_2CO_3$	Yes	Precursor	35	0.3	—	—	—	—
		Yes	Calcined	30	0.3	—	—	16	28
		N/A		28	0.3	8.8	18.1	6	10
	Na_2CO_3	Yes	Calcined	56	0.7	—	—	21	34
		N/A		16	0.15	13.6	9.7	3	5
Zincian malachite/ aurichalcite	Na_2CO_3	Yes	Precursor	27	0.3	—	—	—	—
		Yes	Calcined	29	0.3	—	—	18	29

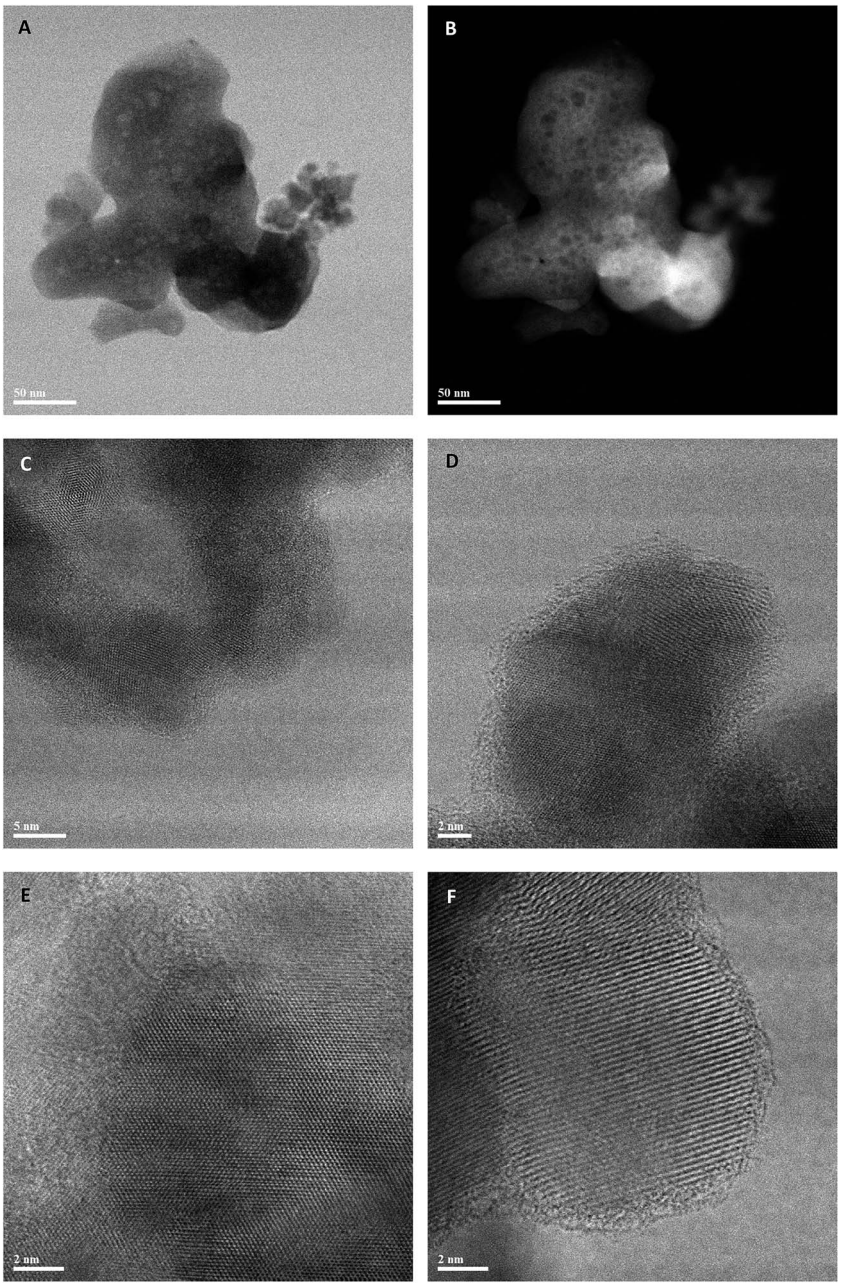

Fig. 7 Representative BF-STEM (A, C, D, E, F) and HAADF-STEM (B) images of the zincian georgeite material prepared by co-precipitation using $(NH_4)_2CO_3$ after calcination at 300 °C.

magnification images such as those in Fig. 7A and B show rounded 200 nm scale agglomerates, in which a considerable amount of residual mesoporosity is evident. Higher-magnification imaging of these particles (Fig. 7C–F) reveal that, after much of the carbonate and hydroxyl content is lost by calcination, most of the disordered matrix material in the precursor has crystallized, and only a small amount of amorphous material remains. The crystallized material is entirely in a nanocrystalline form, with a mean grain diameter of 3–10 nm. Analysis of the fringe spacings and interplanar angles from individual grains suggests that the material is now mainly an intimate mixture of zinc and copper oxides; the small amount of disordered material corresponds to the residual occluded carbonate material, as detected (see below) by TGA/EGA analysis of this material. In comparison, imaging of zincian malachite after calcination determined a copper oxide and zinc oxide matrix extending around pores with much longer range crystalline order (ESI Fig. S5A and B†) than the corresponding calcined co-precipitated zincian georgeite materials.

TGA and DTA was carried out to derive a better understanding of the processes at play during calcination (Fig. 8). Total mass losses measured for zincian georgeite by TGA were between 29–32% with *ca.* 12% residual mass retained after 300 °C (Fig. 8A). Evolved gas analysis (EGA) determined the first

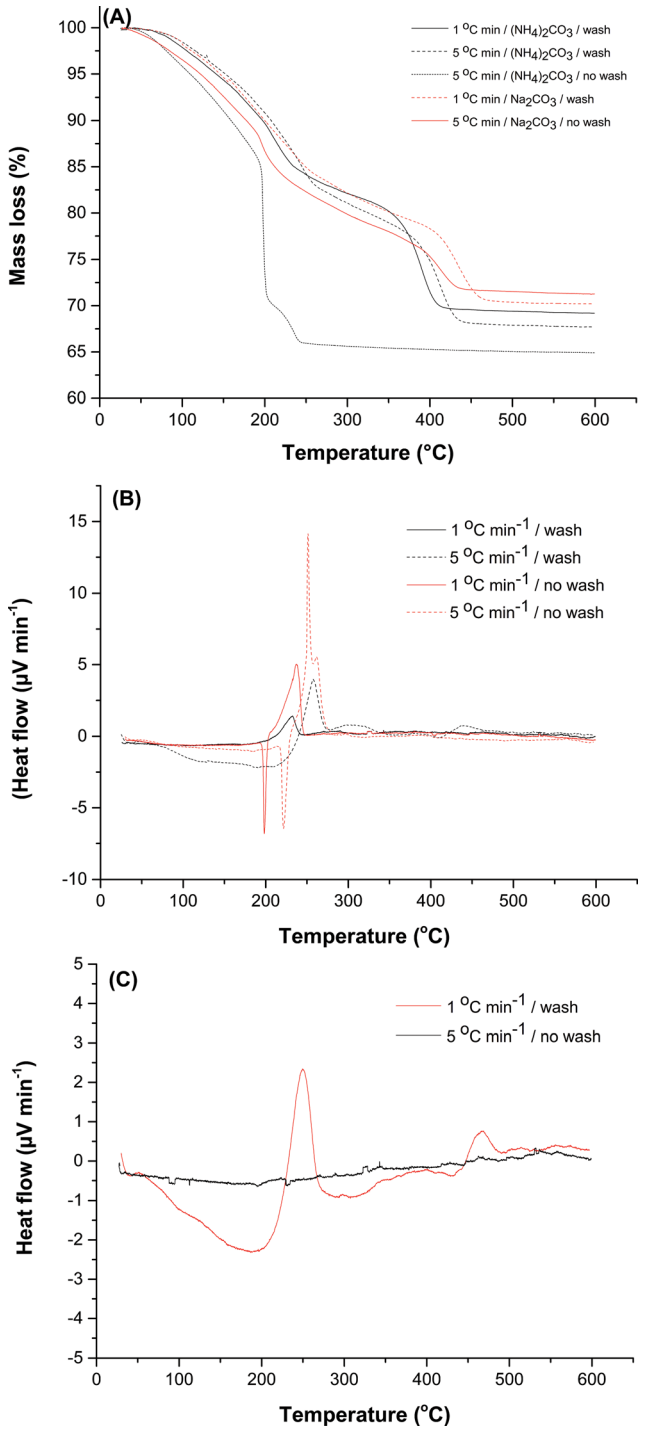

Fig. 8 (A) TGA illustrating effect of precipitation reagent, washing treatment and ramp rate on the thermal decomposition of zincian georgeite. DTA illustrating effect of ramp rate and washing treatment on the thermal decomposition of zincian georgeite prepared using (B) $(NH_4)_2CO_3$ and (C) Na_2CO_3.

weight loss to occur between 100–200 °C and was associated with a simultaneous release of CO_2 ($m/z = 44$) and H_2O ($m/z = 18$), whilst the mass loss at temperatures >350 °C was exclusively due to loss of CO_2 (ESI Fig. 6†). This final mass loss is attributed to the presence of a high temperature carbonate phase ($HT\text{-}CO_3$). For zincian georgeite samples prepared using $(NH_4)_2CO_3$, small amounts of NO_x ($m/z = 30$ and 46) being emitted were also detected. The TGA profile also indicated that there was no $HT\text{-}CO_3$ decomposition step, with total decomposition apparent after 245 °C, for the unwashed material prepared using $(NH_4)_2CO_3$ (Fig. 8A). Analysis of the DTA profiles indicated that this was associated with a highly exothermic decomposition (Fig. 8B). Similar findings were obtained using $(NH_4)HCO_3$ as the precipitant (ESI Fig. 7†). We attribute this to the presence of ammonium acetate retained as a by-phase from the synthesis procedure, as also indicated by FT-IR and Raman spectroscopy (Fig. 1 and ESI Fig. 2†). Washing is beneficial directly after co-precipitation because it reduces the amount of ammonium acetate retained in the zincian georgeite. The exothermic decomposition of this phase upon calcination facilitates sintering of the metal oxide crystallites and removal of the $HT\text{-}CO_3$ component. This effect can also be suppressed from using lower ramp rates during heating cycles or by carrying out thermal treatment under nitrogen (ESI Fig. 8†). It has also been widely reported that the retention of residual carbonates after calcination promotes the performance of the final catalyst.[29,42,45–48] In particular, residual carbonates could suppress sintering during Cu crystallite formation in the subsequent exothermic reduction step. The Cu surface area was found to increase from 6 to 16 $m^2\ g^{-1}$ due to the $HT\text{-}CO_3$ being retained after calcination. However, washing showed a negligible effect on the physical properties on the calcined material (Fig. 5B and Table 4). Loss of $HT\text{-}CO_3$ could result in an improved porous structure despite larger metal oxide crystallites being present. Surprisingly when using Na_2CO_3 as the precipitant for preparing the zincian georgeite, washing did not dramatically influence either the TGA or DTA profile (Fig. 8C). $HT\text{-}CO_3$ was present in both cases with the decompositions being relatively thermo-neutral. The formation of larger metal crystallites after calcination from the absence of washing is therefore more difficult to address. It was noted however that using $(NH_4)_2CO_3$ resulted in the complete removal of the acetate by-phase after calcination and the formation of high purity catalysts. This did not apply when using Na_2CO_3, since sodium is still present on the final catalyst.

Therefore CO_2-TPD was also carried out on the final catalysts to examine the role of Na^+ (Fig. 9). Analysis was first carried out without CO_2 exposure in order to identify features that were not associated with desorbed CO_2. Interestingly, a very small peak was present at temperatures ≥280 °C which will be masked by signals in this higher temperature range. We attribute this signal to residual carbonate still present after reduction, with the peak maximum centred at 438 °C. The majority of profiles display a low temperature peak centred at 96 °C, and a much broader doublet centred at 331 and 380 °C. Similar findings have been reported elsewhere, with the former being assigned to desorption from metallic Cu and the latter to that from ZnO.[40] CO_2 removed at 96 °C would be labile in our testing carried out at temperatures ≥190 °C. However, for the catalyst prepared using Na_2CO_3 without washing a slightly different profile is apparent, with an additional peak at 178 °C. Interestingly, this peak is absent when the material is washed,

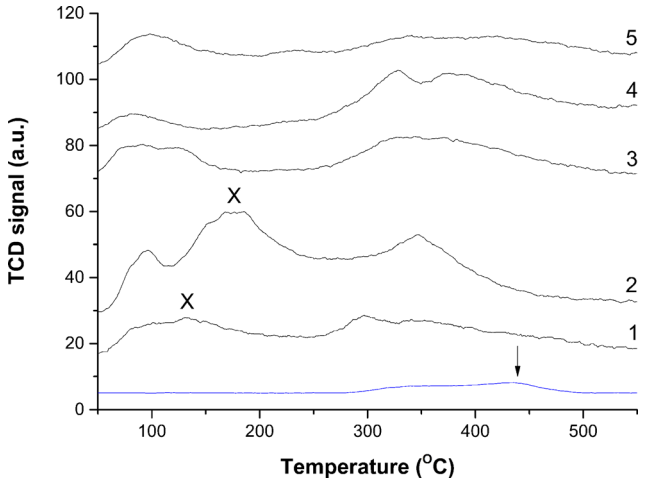

Fig. 9 Effect of precipitation reagent and washing on CO_2-TPD profiles of zincian georgeite derived catalysts. Na_2CO_3 (1) washed and (2) not washed. $(NH_4)_2CO_3$ (3) washed and (4) not washed. Comparisons were made against the zincian malachite derived catalyst (5). Selected peaks at 178 °C and 132 °C are marked for clarity (X) (see main text). The blue line represents (3) without CO_2 exposure, with an arrow indicating a peak maximum apparent at 438 °C.

although another low intensity peak appears at 132 °C. This could be attributed to the stronger binding of the CO_2 molecule to the catalyst surface because of Na^+, requiring additional energy for its desorption. Consequently, Na^+ may play a more influential role in the LTS reaction because a high surface coverage of CO_2 as product would block active sites. This is unfortunate since the optimum microstructural properties were associated with materials derived from using Na_2CO_3 followed by washing (Table 4). Furthermore, the TGA findings indicated that the temperature required for complete HT-CO_3 decomposition was highest for this material (Fig. 8A). Washing resulted in this decomposition temperature shifting from 440 °C to 465 °C. In comparison, the highest temperature for total HT-CO_3 removal for the $(NH_4)_2CO_3$ prepared materials was also 440 °C. This temperature could therefore be correlated to the dispersion of Cu and Zn in the materials and thus may provide a useful methodology for screening catalysts. Simultaneous formation of a copper–ammine complex in the mother liquor could disrupt the co-precipitation process and result in inferior materials when using $(NH_4)_2CO_3$. Regardless, this reagent enables high purity Cu/ZnO catalysts to be prepared without the retention of catalytic poisons.

Conclusions

We have shown that zincian georgeite can be readily prepared by co-precipitation, but the resultant material was found to contain more impurities, together with a slightly more ordered structure than the comparable material prepared by the SAS precipitation method.[36] However, the co-precipitated zincian georgeite derived catalyst still displayed superior performance for methanol synthesis and the LTS reaction in comparison to a conventional zincian malachite derived catalyst. Even though the zincian georgeite made from co-precipitation produces a catalyst with a slightly poorer performance than those derived from SAS precipitation, the same general structural and physical characteristics were observed in both. We correlated the high activity of zincian georgeite derived catalysts to a number of key features. Firstly, the desired porous mesostructure found in an optimised zincian malachite catalyst precursor can also be obtained from zincian georgeite. Secondly, washing directly after co-precipitation strongly influences the properties of this mesostructure, whilst the presence of Na^+ was found to be detrimental. Thirdly, retention of some residual carbonates and poor structural order after calcination are also pivotal in the preparation of highly active catalysts. This achieves metal oxide crystallites $\leq$5 nm in size that are highly dispersed and stabilised in a carbonate matrix prior to reduction. Furthermore, careful selection of the starting reagents enables preparation of high purity catalysts, devoid of any catalytic poisons.

Acknowledgements

We would like to thank the UK Catalysis Hub, Engineering and Physical Sciences Research Council (grants EP/K014714/1, EP/K014714/1, EP/K014668/1, EP/K014706/1, EP/I019693/1), and Johnson Matthey for financial support. We would like to acknowledge the use of the Diamond light source for access to beamline I15 that contributed to the PDF results. This research used resources of the Advanced Photon Source, a U.S. Department of Energy (DOE) Office of Science User Facility operated for the DOE Office of Science by Argonne National Laboratory under Contract No. DE-AC02-06CH11357. We thank Karena Chapman for the collection of PDF data at beamline 11-ID-B, APS. CJK gratefully acknowledges funding from the National Science Foundation Major Research Instrumentation program (GR# MRI/DMR-1040229).

References

1 M. Behrens and R. Schlogl, *Z. Anorg. Allg. Chem.*, 2013, **639**, 2683–2695.
2 R. J. Madon, D. Braden, S. Kandoi, P. Nagel, M. Mavrikakis and J. A. Dumesic, *J. Catal.*, 2011, **281**, 1–11.
3 C. Rhodes, G. J. Hutchings and A. M. Ward, *Catal. Today*, 1995, **23**, 43–58.
4 M. Behrens, F. Studt, I. Kasatkin, S. Kuhl, M. Havecker, F. Abild-Pedersen, S. Zander, F. Girgsdies, P. Kurr, B. L. Kniep, M. Tovar, R. W. Fischer, J. K. Norskov and R. Schlogl, *Science*, 2012, **336**, 893–897.
5 M. Behrens, *Angew. Chem., Int. Ed.*, 2014, **53**, 12022–12024.
6 T. Lunkenbein, J. Schumann, M. Behrens, R. Schlogl and M. G. Willinger, *Angew. Chem., Int. Ed.*, 2015, **54**, 4544–4548.
7 M. V. Twigg and M. S. Spencer, *Top. Catal.*, 2003, **22**, 191–203.
8 C. Baltes, S. Vukojevic and F. Schuth, *J. Catal.*, 2008, **258**, 334–344.
9 O. Martin and J. Perez-Ramirez, *Catal. Sci. Technol.*, 2013, **3**, 3343–3352.

10 M. Kurtz, H. Wilmer, T. Genger, O. Hinrichsen and M. Muhler, *Catal. Lett.*, 2003, **86**, 77–80.
11 F. Arena, G. Mezzatesta, G. Zafarana, G. Trunfio, F. Frusteri and L. Spadaro, *J. Catal.*, 2013, **300**, 141–151.
12 M. Behrens, S. Zander, P. Kurr, N. Jacobsen, J. Senker, G. Koch, T. Ressler, R. W. Fischer and R. Schlogl, *J. Am. Chem. Soc.*, 2013, **135**, 6061–6068.
13 J. Schumann, M. Eichelbaum, T. Lunkenbein, N. Thomas, M. C. A. Galvan, R. Schlogl and M. Behrens, *ACS Catal.*, 2015, **5**, 3260–3270.
14 B. Bems, M. Schur, A. Dassenoy, H. Junkes, D. Herein and R. Schlogl, *Chem.–Eur. J.*, 2003, **9**, 2039–2052.
15 A. M. Pollard, M. S. Spencer, R. G. Thomas, P. A. Williams, J. Holt and J. R. Jennings, *Appl. Catal., A*, 1992, **85**, 1–11.
16 M. Behrens, *J. Catal.*, 2009, **267**, 24–29.
17 M. S. Spencer, *Top. Catal.*, 1999, **8**, 259–266.
18 B. L. Kniep, T. Ressler, A. Rabis, F. Girgsdies, M. Baenitz, F. Steglich and R. Schlogl, *Angew. Chem., Int. Ed.*, 2004, **43**, 112–115.
19 E. N. Muhamad, R. Irmawati, Y. H. Tautiq-Yap, A. H. Abdullah, B. L. Kniep, F. Girgsdies and T. Ressler, *Catal. Today*, 2008, **131**, 118–124.
20 S. Zander, B. Seidlhofer and M. Behrens, *Dalton Trans.*, 2012, **41**, 13413–13422.
21 A. A. Mirzaei, H. R. Shaterian, R. W. Joyner, M. Stockenhuber, S. H. Taylor and G. J. Hutchings, *Catal. Commun.*, 2003, **4**, 17–20.
22 A. A. Mirzaei, H. R. Shaterian, S. H. Taylor and G. J. Hutchings, *Catal. Lett.*, 2003, **87**, 103–108.
23 B. L. Kniep, F. Girgsdies and T. Ressler, *J. Catal.*, 2005, **236**, 34–44.
24 H. Jung, D. R. Yang, O. S. Joo and K. D. Jung, *Bull. Korean Chem. Soc.*, 2010, **31**, 1241–1246.
25 D. Waller, D. Stirling, F. S. Stone and M. S. Spencer, *Faraday Discuss. Chem. Soc.*, 1989, **87**, 107–120.
26 M. Behrens, A. Furche, I. Kasatkin, A. Trunschke, W. Busser, M. Muhler, B. Kniep, R. Fischer and R. Schlogl, *ChemCatChem*, 2010, **2**, 816–818.
27 M. Behrens, S. Kissner, F. Girsgdies, I. Kasatkin, F. Hermerschmidt, K. Mette, H. Ruland, M. Muhler and R. Schlogl, *Chem. Commun.*, 2011, **47**, 1701–1703.
28 M. Behrens and F. Girgsdies, *Z. Anorg. Allg. Chem.*, 2010, **636**, 919–927.
29 A. Budiman, M. Ridwan, S. M. Kim, J. W. Choi, C. W. Yoon, J. M. Ha, D. J. Suh and Y. W. Suh, *Appl. Catal., A*, 2013, **462–463**, 220–226.
30 I. Atake, K. Nishida, D. Li, T. Shishido, Y. Oumi, T. Sano and K. Takehira, *J. Mol. Catal. A: Chem.*, 2007, **275**, 130–138.
31 M. J. L. Gines, N. Amadeo, M. Laborde and C. R. Apesteguia, *Appl. Catal., A*, 1995, **131**, 283–296.
32 P. J. Bridge, J. Just and M. H. Hey, *Mineral. Mag.*, 1979, **43**, 97–98.
33 A. M. Pollard, R. G. Thomas, P. A. Williams, J. Just and P. J. Bridge, *Mineral. Mag.*, 1991, **55**, 163–166.
34 M. A. J. Hartig, N. Jacobsen and W. Peukert, *Chem. Eng. Sci.*, 2014, **109**, 158–170.
35 M. A. J. Hartig, W. Peukert, N. Jacobsen and A. Leuthold, *AIChE J.*, 2015, **61**, 2104–2116.
36 S. A. Kondrat, P. J. Smith, P. P. Wells, P. A. Chater, J. H. Carter, D. J. Morgan, E. M. Fiordaliso, J. B. Wagner, T. E. Davies, L. Lu, J. K. Bartley, S. H. Taylor, M. S. Spencer, C. J. Kiely, G. J. Kelly, C. W. Park, M. J. Rosseinsky and G. J. Hutchings, *Nature*, 2016, **531**, 83–87.
37 G. Prieto, K. P. de Jong and P. E. de Jongh, *Catal. Today*, 2013, **215**, 142–151.
38 G. Simson, E. Prasetyo, S. Reiner and O. Hinrichsen, *Appl. Catal., A*, 2013, **450**, 1–12.
39 J. G. Wu, S. C. Luo, J. Toyir, M. Saito, M. Takeuchi and T. Watanabe, *Catal. Today*, 1998, **45**, 215–220.
40 K. W. Jun, W. J. Shen, K. S. R. Rao and K. W. Lee, *Appl. Catal., A*, 1998, **174**, 231–238.
41 K. C. Waugh, *Catal. Today*, 1992, **15**, 51–75.
42 M. Behrens, F. Girgsdies, A. Trunschke and R. Schlogl, *Eur. J. Inorg. Chem.*, 2009, 1347–1357.
43 R. L. Frost, M. C. Hales and B. J. Reddy, *Polyhedron*, 2007, **26**, 3291–3300.
44 R. L. Frost, W. N. Martens, L. Rintoul, E. Mahmutagic and J. T. Kloprogge, *J. Raman Spectrosc.*, 2002, **33**, 252–259.
45 M. Schur, B. Bems, A. Dassenoy, I. Kassatkine, J. Urban, H. Wilmes, O. Hinrichsen, M. Muhler and R. Schlogl, *Angew. Chem., Int. Ed.*, 2003, **42**, 3815–3817.
46 P. Kowalik, M. Konkol, K. Antoniak, W. Prochniak and P. Wiercioch, *J. Mol. Catal. A: Chem.*, 2014, **392**, 127–133.
47 G. J. Millar, I. H. Holm, P. J. R. Uwins and J. Drennan, *J. Chem. Soc., Faraday Trans.*, 1998, **94**, 593–600.
48 S. Fujita, S. Moribe, Y. Kanamori, M. Kakudate and N. Takezawa, *Appl. Catal., A*, 2001, **207**, 121–128.